Supplementary Information

Dramatic impact of the TiO_2 polymorph on the electrical properties of 'stoichiometric' $Na_{0.5}Bi_{0.5}TiO_3$ ceramics prepared by solid-state reaction

Fan Yang[1,#,*], Yidong Hu[2,#], Qiaodan Hu[2,*], Sebastian Steiner[3], Till Frömling[3,*], Linhao Li[4], Patrick Wu[4], Emilio Pradal-Velázquez[4] and Derek C Sinclair[4,*]

[1] Institute of Fuel Cells, School of Mechanical Engineering, Shanghai Jiao Tong University, 800 Dongchuan Road, Minhang District, Shanghai, 200240, P. R. China.

[2] School of Materials Science and Engineering, Shanghai Jiao Tong University, 800 Dongchuan Road, Minhang District, Shanghai, 200240, P. R. China

[3] Department of Materials and Earth Science, Technical University of Darmstadt, FB Nichtmetallisch-Anorganische Werkstoffe, Alarich-Weiss-Straße 2, D-64287 Darmstadt, Germany

[4] Department of Materials Science and Engineering, University of Sheffield, Sir Robert Hadfield Building, Mappin Street, Sheffield, S1 3JD, UK.

*Corresponding authors.

fanyang_0123@sjtu.edu.cn; qdhu@sjtu.edu.cn; froemling@ceramics.tu-darmstadt.de; d.c.sinclair@sheffield.ac.uk

# Equally contributed authors.

1. Comparison of the electrical conductivity of NBT ceramics sintered with and without binder

Here two methods were used to sinter dense NBT ceramics, including 1) uni-axial cold pressing followed by isostatic pressing at 200 MPa (denoted as "cip") and 2) uni-axial pressing with a 5 wt.% water solution of polyvinyl alcohol (PVA) as binder without isostatic pressing (denoted as "binder"). Fig.S1 compares the bulk conductivity (σ_b) of Bi-deficient NBT ($NB_{0.49}T$), nominally stoichiometric NBT ($NB_{0.50}T$) and Bi-excess NBT ($NB_{0.51}T$) prepared by the above two methods. These ceramics were all prepared using rutile TiO_2. Fig.S1 shows use of binder causes a slight decrease of σ_b of $NB_{0.50}T$ without changing the σ_b -1000/T relationship. The two sintering methods do not cause the significantly different electrical conductivity of $NB_{0.50}T$ prepared using rutile and anatase TiO_2, and therefore do not influence the major conclusion of this work.

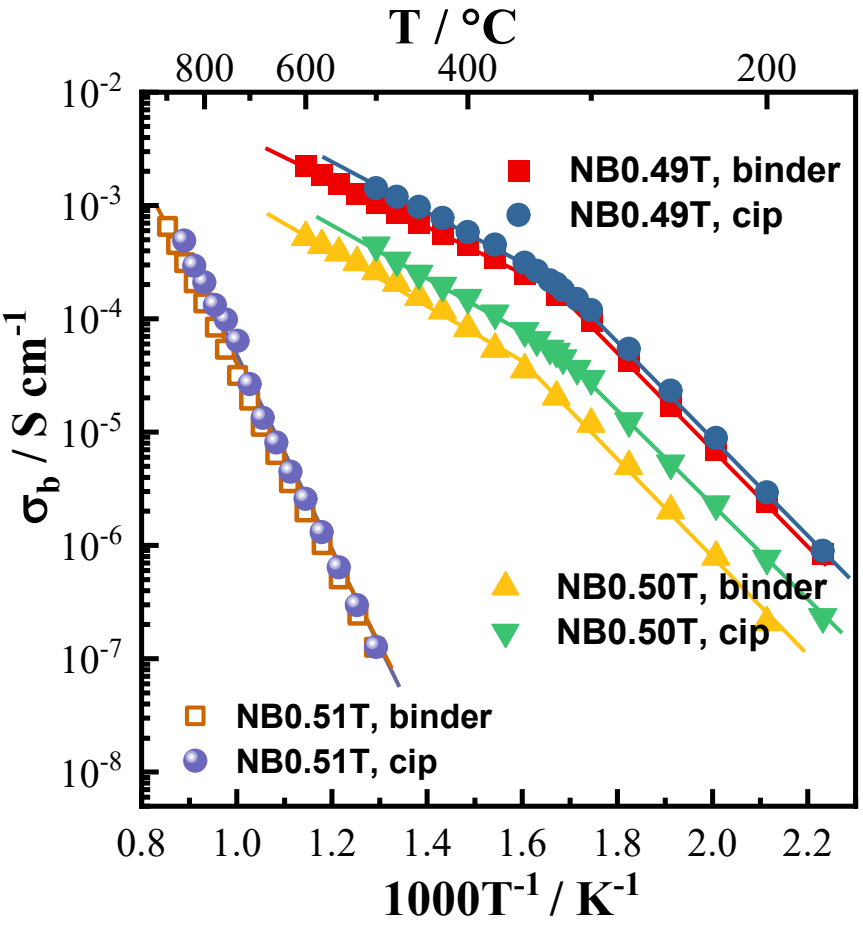

Figure S1. Arrhenius plots for σ_b of Bi-deficient NBT ($NB_{0.49}T$), nominally stoichiometric NBT ($NB_{0.50}T$) and Bi-excess NBT ($NB_{0.51}T$). All ceramics were prepared by rutile TiO_2. "cip" represents uni-axial cold pressing followed by isostatic pressing. "binder" represents uni-axial cold pressing with PVA as a binder without isostatic pressing.

2. XRD patterns of NBT ceramics prepared from different reagents

Fig.S2 shows the XRD patterns of NBT ceramics prepared by different reagents. The numbers after NBT represent different combinations of Na_2CO_3, Bi_2O_3 and TiO_2 reagents from Table 1 in the main text. All NBT ceramics are phase pure with a rhombohedral structure.

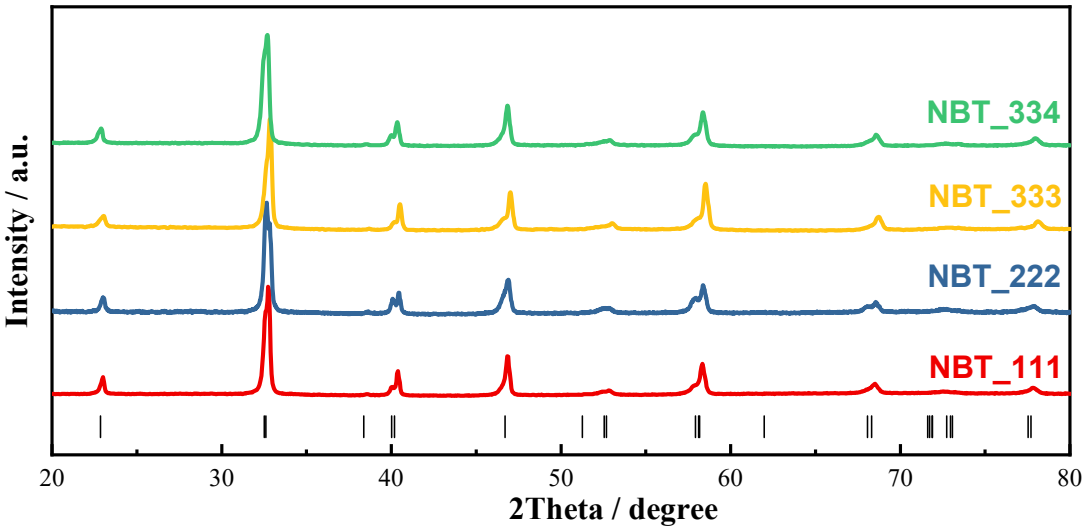

Figure S2. XRD patterns of sintered NBT ceramics prepared by different reagents. The vertical lines below the patterns represent the peak positions for NBT with a rhombohedral structure.

3. Full synchrotron XRD patterns in the 2θ range between 15-85°

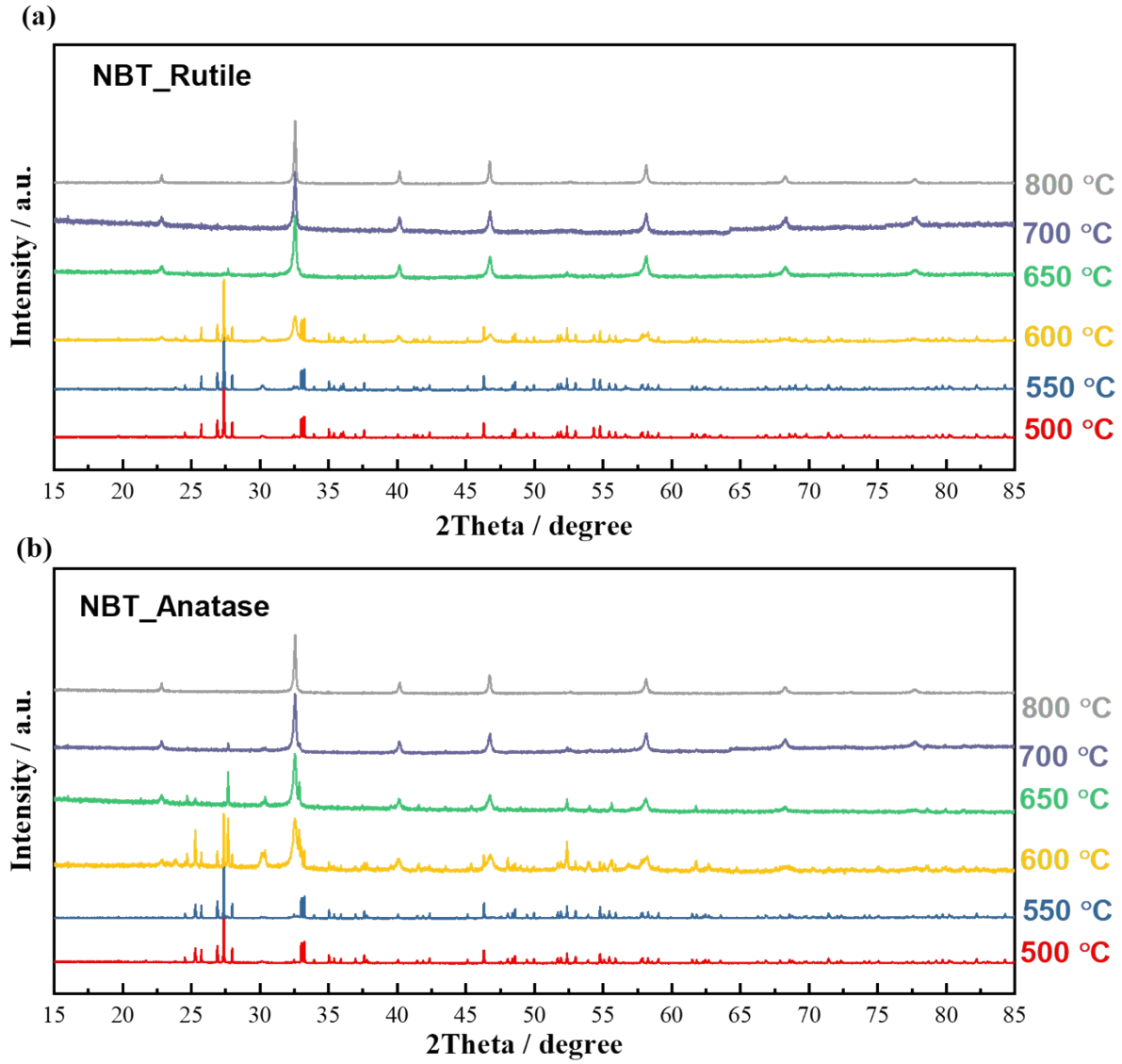

Figure S3. Evolution of the XRD patterns with calcination temperature in the 2θ range between 15-85. (a) Mixture with rutile TiO_2 and (b) with anatase TiO_2.

4. Particle size distribution

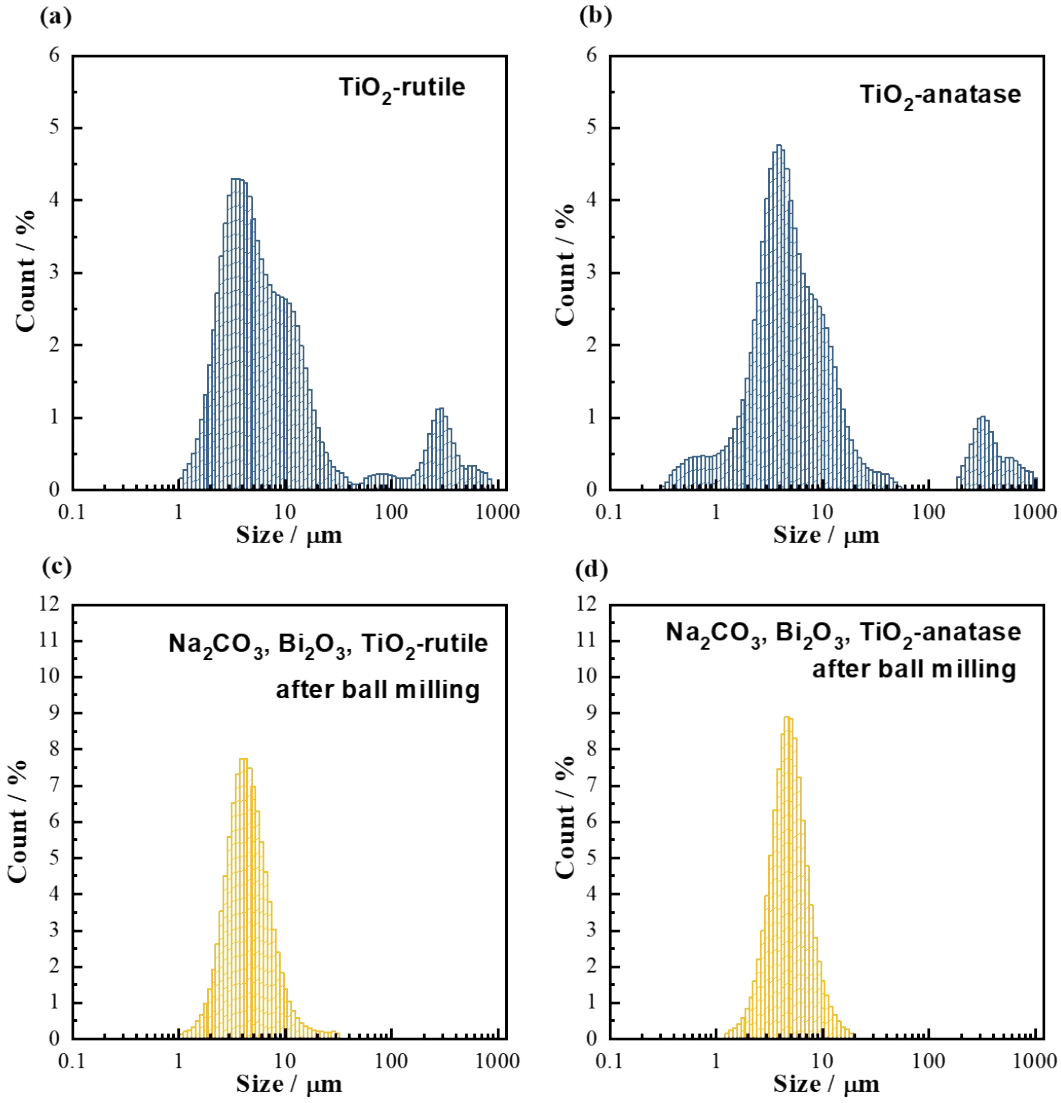

Figure S4. Particle size distribution of (a) raw rutile TiO_2, (b) raw anatase TiO_2, (c) ball-milled and sieved mixture of pre-dried Na_2CO_3, Bi_2O_3 and rutile TiO_2, and (d) ball-milled and sieved mixture of Na_2CO_3, Bi_2O_3 and anatase TiO_2.

5. Evolution of Bi_2O_3, $Bi_{12}TiO_{20}$ and NBT fractions during solid-state reaction

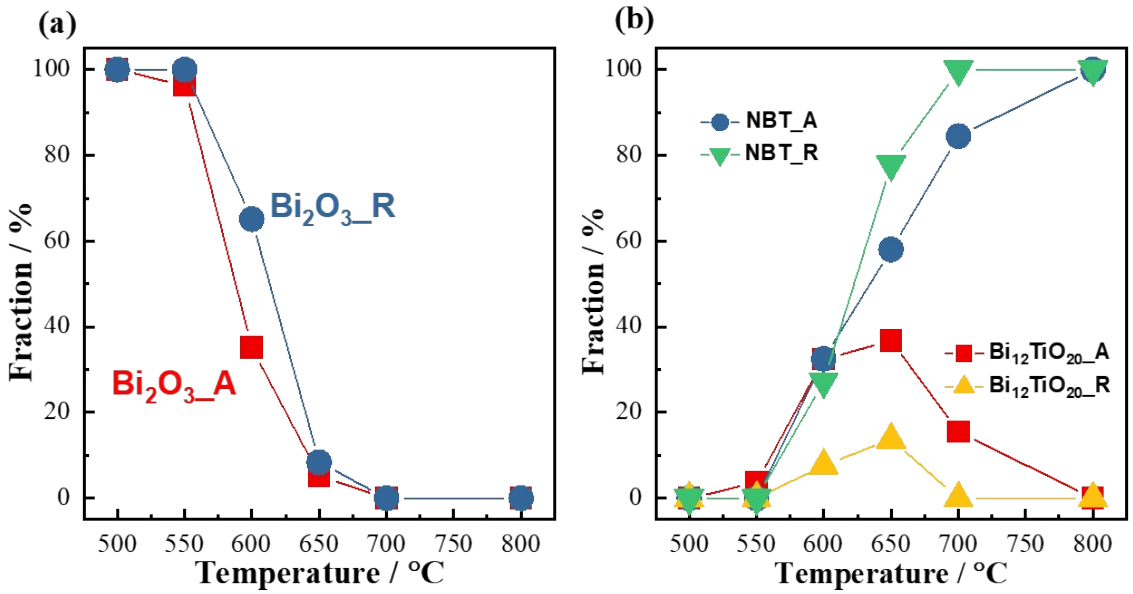

Figure S5. Evolution of the fraction parameter of Bi-containing phases during solid-state reaction when rutile and anatase TiO_2 are used as reagents. (a) Bi_2O_3, (b) $Bi_{12}TiO_{12}$ and NBT.

6. Impedance spectroscopy of NBT_$R_{0.5}A_{0.5}$

Impedance data for NBT_$R_{0.5}A_{0.5}$ are presented in Nyquist (Fig.S6a) and Bode (M''-log*f*, Fig.S6b) plots. Z* plots for NBT_$R_{0.5}A_{0.5}$ at 500 °C show two poorly resolved arcs and a low-frequency spike corresponding to an electrode effect. The electrode spike is characteristic of ionic conduction behavior. With increasing temperature, the two arcs gradually merge into one suggesting a different activation energy for the two responses. M''-log*f* plots at lower temperatures, e.g., 300 °C, show a broad peak, suggesting an inhomogeneous electrical microstructure for NBT_$R_{0.5}A_{0.5}$. The M''-log*f* peak height increases with increasing temperature suggesting a reduced relative permittivity with increasing temperature between 300 – 700 °C. The inhomogeneous electrical microstructure agrees with the random distribution of large and small grains, as shown in Fig.6c.

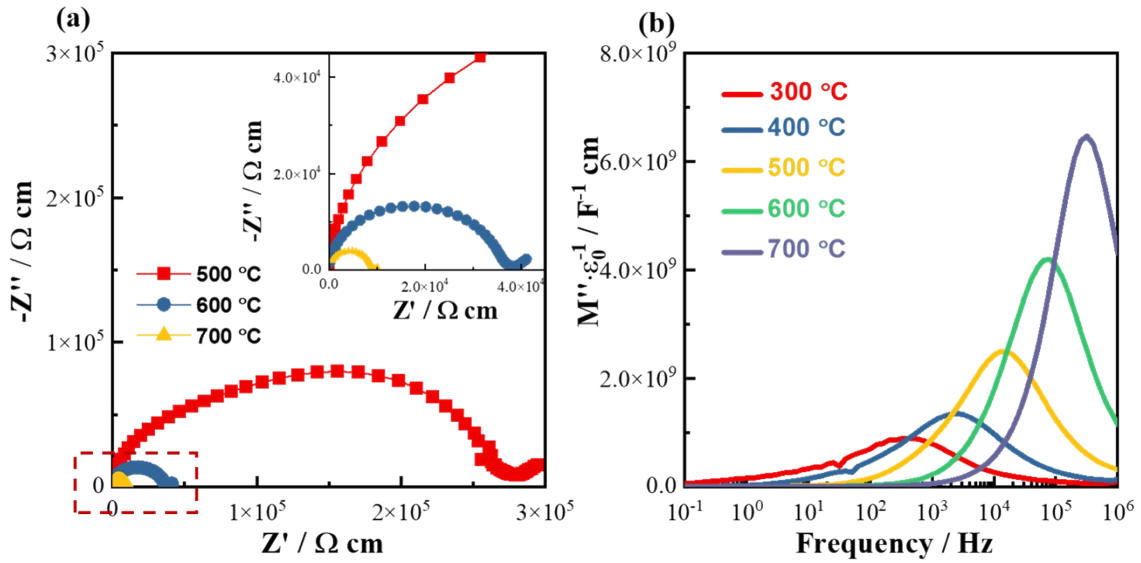

Figure S6. Impedance data for NBT_$R_{0.5}A_{0.5}$. (a) Z* plots at 500, 600 and 700 °C and (b) M''-log*f* plots at 300-700 °C at increments of 100 °C. The inset figure in (a) is an expanded view of the rectangular region.